

# A Pilot Survey for KX QSOs in the UKIDSS Ultra Deep Survey Field

Ian Smail,<sup>1\*</sup> Rob Sharp,<sup>2</sup> A. M. Swinbank,<sup>1</sup> M. Akiyama,<sup>3</sup> Y. Ueda<sup>4</sup> S. Foucaud,<sup>5</sup> O. Almaini,<sup>5</sup> S. Croom<sup>6</sup>

<sup>1</sup>*Institute for Computational Cosmology, Department of Physics, Durham University, South Road, Durham, DH1 3LE, UK*

<sup>2</sup>*Anglo-Australian Observatory, Epping, NSW 1710, Australia*

<sup>3</sup>*Subaru Telescope, National Astronomical Observatory of Japan, 650 North A'ohoku Place, Hilo, HI 96720, USA*

<sup>4</sup>*Department of Astronomy, Kyoto University, Kyoto 606-8502, Japan*

<sup>5</sup>*School of Physics and Astronomy, University of Nottingham, University Park, Nottingham NG7 2RD*

<sup>6</sup>*School of Physics, University of Sydney, NSW 2006, Australia*

\**Email: ian.smail@durham.ac.uk*

Accepted 2008 June 16. Received 2008 June 13; in original form 2008 March 9

## ABSTRACT

We have undertaken a pilot survey for faint QSOs in the UKIDSS Ultra Deep Survey Field using the KX selection technique. These observations exploit the very deep near-infrared and optical imaging of this field from UKIRT and Subaru to select candidate QSOs based on their  $VJK$  colours and morphologies. We determined redshifts for 426 candidates using the AAOmega spectrograph on the AAT in service time. We identify 17 QSOs ( $M_B \lesssim -23$ ) in this pilot survey at  $z = 1.57\text{--}3.29$ . We combine our sample with an X-ray selected sample of QSOs in the same field (a large fraction of which also comply with our KX selection) to constrain the surface density of QSOs with  $K \leq 20$ , deriving limits on the likely surface density of 85–150  $\text{deg}^{-2}$ . We use the good image quality available from our near-infrared imaging to detect a spatially extended component of the QSO light which probably represents the host galaxies. We also use our sample to investigate routes to improve the selection of KX QSOs at faint limits in the face of the significant contamination by compact, foreground galaxies. The brightest examples from our combined QSO sample will be used in conjunction with a large VLT VIMOS spectroscopic survey of high redshift galaxies in this region to study the structures inhabited by gas, galaxies and growing super-massive black holes at high redshifts in the UKIDSS UDS.

**Key words:** galaxies: active – quasars: general.

## 1 INTRODUCTION

Simulations of the distribution of baryons in the Universe predict that much material is spread out in a “cosmic web” between the galaxies, groups and larger structures visible in conventional surveys. The main components of this material are the Ly $\alpha$  forest, which traces highly ionized hydrogen of low neutral column density and low chemical enrichment distributed through the lower density regions, and metal absorption lines which trace massive galaxy halos (and hence higher density regions) via their metal-enriched gas. To probe this material and investigate its 3-dimensional distribution we must exploit QSOs as bright background sources to trace the web through its absorption.

An optimal survey of the cosmic web would use a grid of distant bright QSOs as probes of the intervening matter,

with the redshift and equivalent width of these absorbers providing information on the relative distribution and clustering of gas around galaxies and larger structures, as well as providing insights into the chemical enrichment and heating of this material (e.g. Morris & Januzzi 2006). Studies comparing the results from high-redshift galaxy surveys around individual bright QSOs have provided unique insights into the effect of star formation on the gas surrounding young galaxies (e.g. Adelberger et al. 2005). However, these studies are observationally expensive – it would be much more efficient if a large number of galaxies and QSOs could be compared within a single field as the number of absorber–galaxy pairs scales as  $N^2$ . The difficulty is that the surface density of bright QSOs is low and hence faint QSOs are required to set up a dense grid of probes needed to sample the

full range of cosmic structures in a single field (Prescott et al. 2006). Nevertheless, with enough QSOs in a single field the long integration time required to undertake absorption-line analysis on relatively faint background sources (AGN or galaxies) become worthwhile.

We are undertaking a highly-sampled survey of the cosmic web in a uniquely well-studied field: the UKIDSS (Lawrence et al. 2007) Ultra Deep Survey (UDS) field. The UDS is the deepest, panoramic near-infrared observations so far undertaken with the goal of reaching  $K \sim 23$  and  $J \sim 25$  over  $\sim 0.8$  sq. degrees (Foucaud et al. 2007). Equally deep  $BVRIZ$  imaging is available across the whole field from Subaru/XMM Deep Survey (SXDS, Furusawa et al. 2008) and this region has also been extensively studied at X-ray wavelengths as part of the same project (Ueda et al. 2008). These data are being analysed to study the build-up of massive galaxies out to  $z \sim 3$  and its variation with environment (Foucaud et al. 2007; Lane et al. 2007; Cirasulo et al. 2007). This field is also the target of a VLT Large Programme (PI: O. Almaini) to use the VIMOS spectrograph to obtain redshifts for  $\sim 5,000$  high-redshift  $K$ -selected galaxies. In this paper we present a parallel pilot survey to expand the size of the QSO sample in this field to allow us to relate these luminous galaxies and structures to their surrounding enriched and unenriched gas from a highly-sampled grid of sightlines. Combining these two unique datasets will yield powerful insights into the influence of galaxies and AGN (at the peak era in their activity) on low-density gas in their environments, material which is required for the long-term fueling of the star formation in galaxies.

To construct a highly-sampled grid of QSOs in this field we have used  $VJK$ -band imaging from UKIDSS/UDS to apply the KX method (Warren et al. 2000; Croom et al. 2001; Sharp et al. 2002) to identify a sample of  $\sim 800$   $V < 23$  potential AGN candidates in this region. The good seeing available in the UDS imaging,  $0.8''$  FWHM across the whole field, yields relatively clean catalogs of point sources – which are a mix of AGN, stars and compact galaxies. The KX method relies on the power-law shape of AGN continua across the  $VJK$  bands, compared to the  $H$ -band “bump” arising from the opacity minimum in stellar atmospheres, to distinguish between those point sources which are AGN and those which are stars. This color selection has the additional advantage that it provides an unbiased selection of QSOs independent of their dust reddening out to high redshifts (Warren et al. 2000), compared to the classical “UVX” selected samples.

We use a cosmology with  $H_0 = 70 \text{ km s}^{-1}$ ,  $\Omega_M = 0.3$  and  $\Omega_\Lambda = 0.7$  in which  $1''$  corresponds to  $8.2 \text{ kpc}$  at  $z = 2.5$  and  $8.5 \text{ kpc}$  at  $z = 1.5$ . All quoted magnitudes are Vega and as the galactic reddening in our field is low,  $E(B-V) = 0.02$ , we have not applied any extinction corrections to the colours or magnitudes in this paper.

## 2 OBSERVATIONS AND REDUCTION

### 2.1 Photometric Selection

Our sample selection starts from the matched near-infrared/optical catalogue of sources in the UKIDSS UDS field. The near-infrared data come from the UKIDSS Data Release 1 (Warren et al. 2007) and the optical photometry

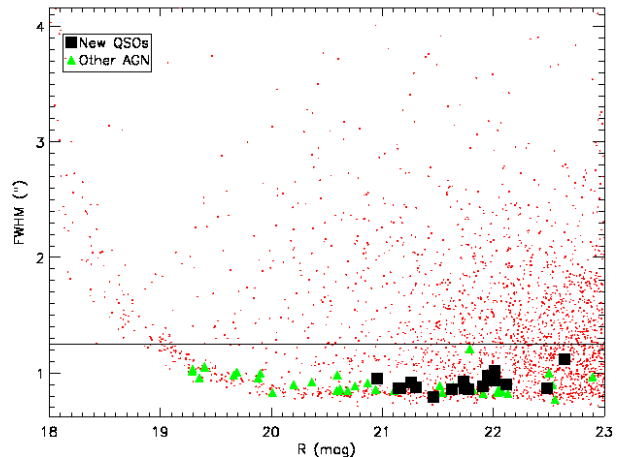


**Figure 1.** A plot of the FWHM in the  $R$ -band versus  $R$ -band magnitude for a random 1-in-3 subset of sources in the UKIDSS UDS. The stellar sequence is visible at  $\sim 0.8''$  (image saturation causes the turn up in the sequence at bright magnitudes). To ensure that we are not biased against QSOs with bright host galaxies or very close companions – we broaden our selection to  $\text{FWHM} \leq 1.25''$ . We also plot the new QSOs identified from our survey, which show a modest range in  $R$ -band FWHM, as well as the existing X-ray selected AGN which comply with our selection and which were used to tune the criteria.

are from an early version of the Subaru catalogues (O. Almaini, priv. comm.) published by Furusawa et al. (2008). The combined catalogue comprises a seeing-matched  $K$ -band selected sample which is then matched to the seeing-matched optical Subaru catalogues (see Furusawa et al. 2008) through the  $i$ -band. The methods used to create this combined optical-near-infrared photometric catalogue are described more fully in Foucaud et al. (2007) and the DR1 catalogue itself is described Almaini et al. (in prep). For our analysis we select only those objects lying in areas with good photometry, without bright neighbours and which are unsaturated/etc, leaving us with over 36,000 objects with  $BVRIZJK$  photometry across a  $0.572 \text{ degree}^2$  field. The  $3\text{-}\sigma$  photometric limit of the catalogue in our key bands are  $V = 27.8$ ,  $R = 27.0$ ,  $J = 23.4$  and  $K = 22.2$ .

In the following we also employ the existing spectroscopic survey of X-ray sources in the SXDF/UDS from Akiyama et al. (2008). This provides a useful sample of known AGN to assess our selection criteria. The Akiyama et al. survey targets the 952 X-ray sources detected either in the  $0.5\text{--}2$  or  $2\text{--}10 \text{ keV}$  bands from the area of the *XMM-Newton* survey of the SXDF (Ueda et al. 2008) which is covered by the deep optical imaging in Furusawa et al. (2008). Of these 952 X-ray sources, 648 have optical counterparts brighter than  $R_{AB} = 24$  in Furusawa et al. (2008). Intensive optical spectroscopic observations of these optical counterparts have been performed with Subaru/FOCAS and VLT/VIMOS and to date  $\sim 60\%$  of the 648 X-ray sources have been spectroscopically identified. The majority of these are moderate redshift AGN, with a tail of QSOs extending

out to beyond  $z \sim 5$ . As we discuss below, in addition to using this catalogue as a training set for our sample selection, we have culled from our catalogue any source with spectroscopy in Akiyama et al., although we have include all the QSOs with  $M_B \leq -23.0$  and brighter than  $K_{tot} = 20.0$  from their survey in our final estimate of the total surface density of QSOs in the  $K$ -band.

We first identify the locus of stars in the FWHM-magnitude plane. We use the Subaru  $R$ -band FWHM for this purpose for two reasons. Firstly, we do not want to bias our selection against QSOs with detectable host galaxies, as these hosts are likely to be redder than the QSOs this argues for using the bluer optical bands in the morphological selection, rather than our near-infrared data. Secondly, the image quality in the  $R$ -band provides the best combination of image quality and depth from our available data. We plot  $R$ -band FWHM versus  $R$ -band magnitude in Fig. 1 and show our  $\text{FWHM} \leq 1.25''$  selection limit. This limit was chosen by comparison to the existing spectroscopic sample in this field, with the aim of yielding a sample well-matched to the grasp of the AAOmega spectrograph with modest contamination. Setting the FWHM limit to  $\leq 1.0''$  yielded a sample of 218 sources complying with our KX-selection (see below). Of these, 43 matched sources in the existing spectroscopically identified catalogue (Akiyama et al. 2008) of which 41 were classified as broad emission line sources (although not all of these have  $M_B \leq -23$ , our definition of a QSO), with just 2 were narrow emission line sources. This selection of AGN thus appeared very pure, but is not necessarily complete and moreover would not fully populate the AAOmega fibres. Extending the FWHM cut to  $\leq 1.25''$  increased the sample of sources with the appropriate colours to 758 (well matched to AAOmega), yielding 89 matches in the existing spectroscopic catalog, from which 47 were broad emission line sources, 21 are narrow emission line sources and the remainder were classified as absorption line spectra. Thus a cut on  $R$ -band FWHM at  $\leq 1.25''$  yielded a sufficiently large sample of KX-selected targets to fill all the AAOmega fibres with a moderate level of contamination (estimated from the existing spectroscopic sample). This relatively relaxed constraint on image size also ensures that we do not reject QSOs in which the host galaxy is detectable.

We then use the  $2''$ -diameter aperture photometry in the  $VJK$  bands to isolate the stellar sequence in colour space (Fig. 2). We limit our sample to  $K_{tot} \leq 22.0$  to ensure completeness in the  $K$ -band catalogue and then required targets complied with:  $V_{ap} \leq 23.0$ ;  $(J - K)_{ap} \geq 1.10$ ;  $(J - K)_{ap} \geq 0.25 * (V - J)_{ap} + 0.40$ . This selection is a variation on that used by Croom et al. (2001), where the changes reflect small differences in the magnitude systems. We note that as our photometric catalogue is seeing-matched, we do not apply any aperture corrections to any of the colours in this paper. We have also ignored the effect of variability on our measured colours and magnitudes, and caution that this may be responsible for throwing QSOs out of our selection. Finally, we also stress that given the typical colours of QSOs,  $(V - K) \sim 2.5$ – $3.5$ , the relatively bright  $V$ -band magnitude limit required by our spectroscopic follow-up means that the QSO sample is effectively limited at  $K \sim 20$  so all have very good  $K$ -band detections,  $> 20\text{-}\sigma$ .

As a final step before our spectroscopic observations, we remove from our sample the 89 objects which are in the

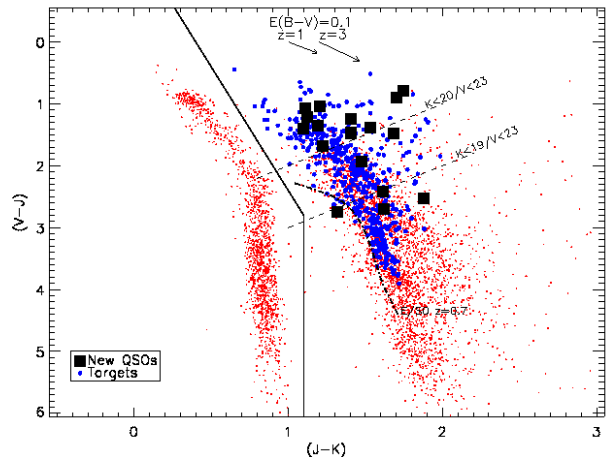


**Figure 2.**  $(V - J)$  versus  $(J - K)$  for objects from the UKIDSS UDS. We plot as the background the distribution of colours for the  $K_{tot} \leq 20.0$  sources in our field. The stellar sequence is clearly visible and can be fairly well separated from the AGN (and compact galaxies) using the colour selections marked. We identify the subset of sources selected on the basis of their morphologies and colours to be targeted for AAOmega spectroscopy and the 17 new QSOs which are identified by this spectroscopy. As can be seen these QSOs are well distributed across the colour plane. We also indicate the potential influence of dust reddening (either intrinsic or from foreground absorption systems) on the colours of QSOs at  $z \sim 1$ – $3$ . We also mark on the selection boundaries (dashed lines) for sources with  $V < 23$  and either  $K < 20$  or  $K < 19$ , and the expected variation in apparent colour of a galaxy with a non-evolving E/S0 SED from  $z = 0$  (top) to  $z = 0.7$  (dot-dashed line).

existing redshift catalog of Akiyama et al. (2008), including their X-ray QSOs which comply with our KX-selection and have  $M_B \leq -23.0$ , which we discuss further in §3.2. After removing these sources we have a final input catalogue comprising 670 targets. In our subsequent spectroscopy we gave priority to sources with  $V < 22.0$  above those with  $V < 22.5$  and  $V < 23.0$ . We model the effects of this variable completeness on our results.

## 2.2 AAOmega Observations

The spectroscopic observations were undertaken as part of the service programme on the Anglo-Australian Telescope (AAT). The total integration time was 6 hrs spread equally over three nights (2006 Aug. 31, Sept. 28 and 2007 July 15). The conditions for the first two runs were good, with seeing  $< 1.5''$  FWHM and good transparency, although the third run suffered from poor seeing,  $3.0''$  FWHM, and yielded few additional redshifts.

Our observations used the AAOmega spectrograph and the multi-object fibre feed from the 2dF fibre positioner system (Saunders et al. 2004; Smith et al. 2004; Sharp et al. 2006). The dual-beam AAOmega spectrograph was used in it's default low resolution configuration, the 580V and 385R

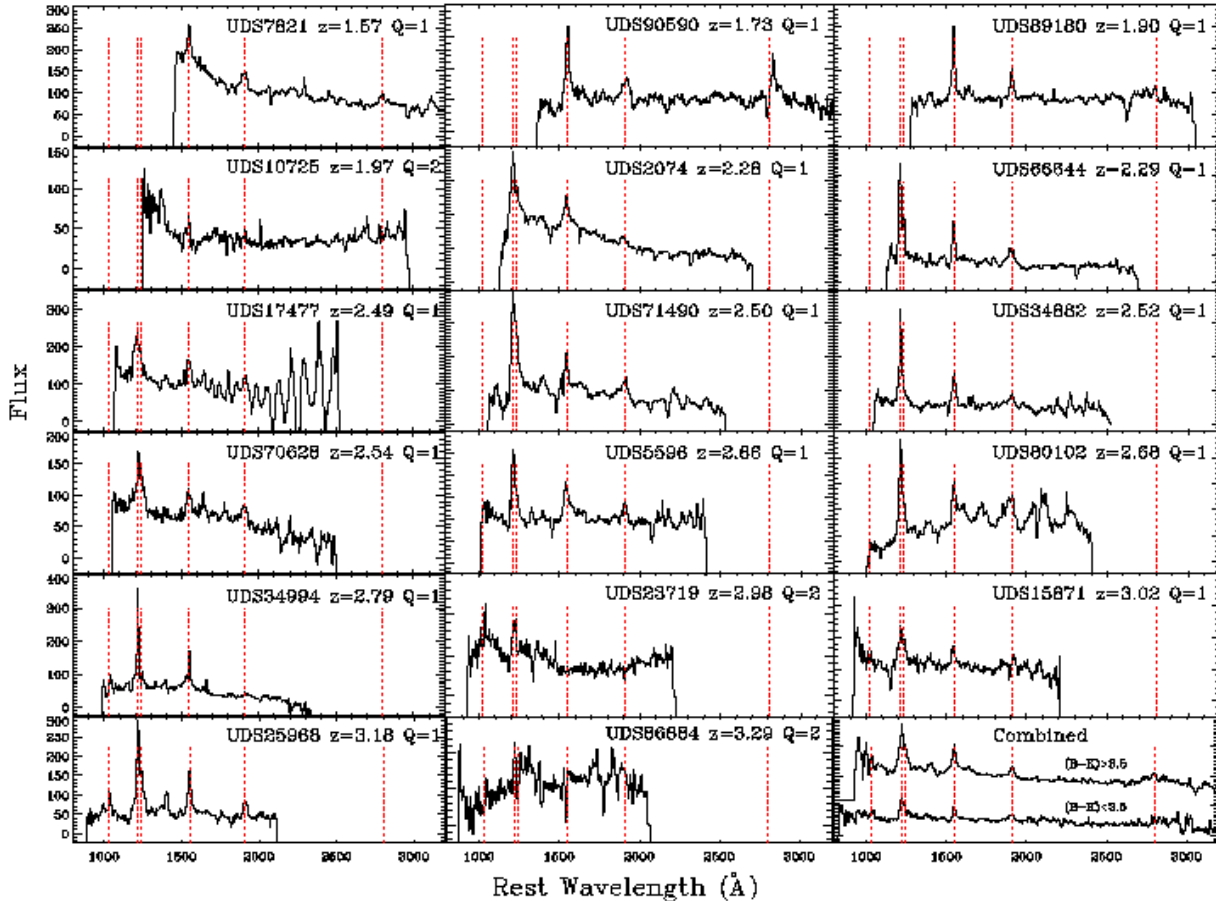


**Figure 3.** Restframe spectra of the 17 new KX-selected QSOs from the AAOmega observations of the UKIDSS/UDS. These are order in increasing redshift (from the upper-left) and have been smoothed with a  $7\text{\AA}$ -FWHM Gaussian for display purposes. In the final panel we show two combined spectra for the redder and bluer QSOs in the sample, divided at  $(B - K) = 3.5$ . We mark on each spectrum the expected wavelengths of common emission features:  $\text{Ly}\beta$   $\lambda 1026$ ,  $\text{Ly}\alpha$   $\lambda 1216$ ,  $\text{Nv}$   $\lambda 1243$ ,  $\text{CIII]}$   $\lambda 1508$  and  $\text{MgII}$   $\lambda 2800$ . The red end of the spectrum of UDS17477 shows interference fringing at the fiber/prism interface on the 2dF fibre positioner. We stress that the spectra have not been accurately flux calibrated (§2.2) and so the continua shape should be treated with caution.

VPH gratings delivering a 3.4 pixel resolution element and  $R \sim 1300$  over the wavelength range  $\lambda = 3700\text{--}8600\text{\AA}$  (the lower limit essentially set by the transmission limit of the 38 meter fibre optic feed, the upper limit constrained by the available CCD coverage). The  $5700\text{\AA}$  dichroic mirror was used to separate the twin beams, the change over occurring in the region  $5700 \pm 200\text{\AA}$ .

The observations were broken up into 2 hour blocks to minimize losses from atmospheric effects<sup>1</sup>. Each observation block consists of a quartz-halogen flat-field exposure (used both to trace fibre footprint on the CCD and also for the relative response of the fibres), a composite arc lamp frame (utilizing CuAr, FeAr hollow cathode arc-lamps and neutral density filtered Helium and Neon lamps) used for primary

wavelength calibration, and four science exposures (each of 1800 s). Twenty five of the  $\sim 370$  fibres available on the 2dF positioner at the time of observation were allocated to sky positions for sky subtraction. These positions were hand-picked from the Subaru imaging. The contemporaneous sky observations are reduced as part of the science fibre reduction, and then combined to make a high signal-to-noise sky spectrum free from cosmic rays and CCD defects for each science exposure.

As is usual for AAOmega observations, the data were processed using the 2DFDR data reduction package<sup>2</sup>. Data from the blue and red arms of the spectrograph are processed independently. In addition to the processing steps common to all fibre spectrograph systems (overscan correction, fibre

<sup>1</sup> For details on these considerations see [http://www.aao.gov.au/AAO/2df/aaomega/aaomega\\_CVD.html](http://www.aao.gov.au/AAO/2df/aaomega/aaomega_CVD.html)

<sup>2</sup> Available from the AAO web site at <http://www.aao.gov.au/AAO/2df/aaomega/aaomega-software.html>



*tramline map* generation, spectral extraction, fibre relative response and wavelength calibration and sky subtraction) 2DFDR implements a Laplace filtering cosmic ray rejection to identify cosmic rays before spectral extraction (van Dokkum 2001) and an iterative sky subtraction involving minimizing the sky subtraction residual by iteratively scaling for: small relative wavelength shifts between the composite sky spectrum and each science spectrum; slight degradation of the science spectrum resolution to match the composite sky; and the intensity of the sky spectrum.

The multiple science spectra for each object are then combined using a weighting derived from the average flux recorded in a subset of the brighter objects in each field (to account for seeing and transparency variations during observation). The blue and red arm data were then spliced together to give a continuous spectrum using an archival transfer function to correct for broad band sensitivity. No detailed flux calibration is attempted. Data from all previous nights were then stacked to build up signal on the fainter targets for which redshift had not been determined. Between each night, all low-redshift ( $z \ll 1$ ) objects for which redshifts were reliably measured were replaced in subsequent observations with alternate targets. This maximized the yield for the final science exposure. In total 626 sources from our candidate catalogue of 670 were observed.

### 3 ANALYSIS, RESULTS AND DISCUSSION

#### 3.1 Spectroscopic Measurements

Redshift determination was performed using the AUTOZ package, which is optimized for measuring QSO redshifts (Croom et al. 2001) and the RUNZ package developed for the 2dFGRS (Colless et al. 2001) and updated for the 2SLAQ project (Cannon et al. 2006). All redshifts were then visually checked. From the 626 objects observed, our spectra yield a total of 426 sources with redshifts of quality (Q) Q=1, unambiguous, or Q=2, probable. Of these 426, 11 are galactic stars: 4 DA white dwarfs, 2 DB white dwarfs and five main sequence stars (one each of A, B, F, G and M). Thus the colour selection from Fig. 2 has significantly reduced, but not totally eliminated, the stellar contamination.

We derive the absolute restframe  $B$ -band magnitudes for these extragalactic sources using KCORRECT (Blanton & Roweis 2007) by interpolating based on a fit to the optical and near-infrared photometry spanning the restframe  $B$ -band. These absolute magnitudes are based on the aperture photometry and so we correct them to total magnitudes using the mean aperture correction for the sample,  $\delta = -0.4 \pm 0.1$ , derived in the  $J$ -band photometry. We then apply a  $M_B \leq -23.0$  cut to identify the QSOs from our spectroscopic sample. This results in 17 QSOs with  $M_B \sim -23.3$  from our AAOmega observations in the UDS which comply with our KX and various image selection criteria. Their redshifts span  $z = 1.57\text{--}3.29$  and we show the spectra for these in Fig. 3 and list their positions and photometric properties in Table 1. The X-ray fluxes in the table come from Ueda et al. (2008) and are in the observed 0.5–4.5 keV band (assuming a power-law photon index of 1.8 with no absorption).

As expected, the spectra of the QSOs in our sample were all best matched with the QSO (broad emission line)

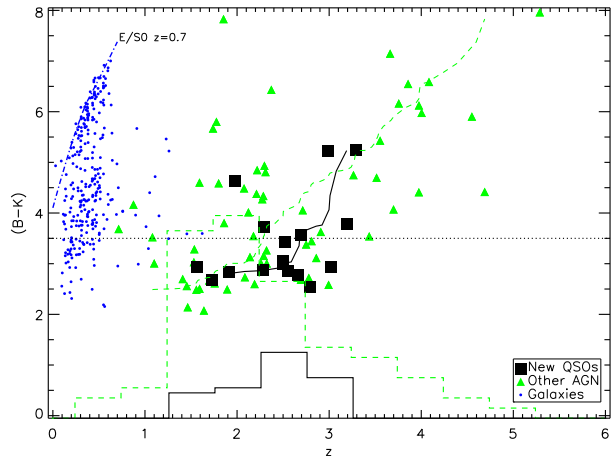


**Figure 4.** The variation in  $(B - K)$  colour as a function of  $z$  for the QSOs in the UDS, as well as the galactic contaminants. We plot the trend in the median colour for the AAOmega KX-sample (solid) and for the X-ray selected QSOs in the field (dashed). For comparison to the galaxy colours we plot the track of a non-evolving E/S0 galaxy ( $z=0.7$ ), which defines the red-envelope of the low-redshift contamination. The horizontal dotted line shows the dividing line for “red” QSOs, with  $(B - K) \geq 3.5$ :  $\sim 35\%$  of the new KX-selected sample are redder than this limit. The histograms at the bottom of the figure show the redshift distribution for the KX-selected QSOs from our AAOmega observations and the existing X-ray selected QSO sample in the UKIDSS UDS field.

template spectrum employed by RUNZ and they typically display broad emission lines, including  $\text{Ly}\alpha$   $\lambda 1216$ ,  $\text{Nv}$   $\lambda 1243$ ,  $\text{Civ}$   $\lambda 1549$ ,  $\text{CIII}]$   $\lambda 1908$  and  $\text{MgII}$   $\lambda 2800$ . In the lower-right panel of Fig. 3 we show the composite spectra formed by combining the individual spectra for the redder and bluer QSOs (divided at  $(B - K) = 3.5$ ) to demonstrate their common features. We note that the redder QSOs show proportionally higher equivalent width emission lines than the blue QSOs. Given the small sample available, this could result from: 1) a selection effect as the bluer QSOs tend to be lower redshift; 2) a selection effect arising from the need for stronger features to be present in the redder QSOs, which are typically fainter in the wavelength range of our AAOmega observations; or 3) absorption and reddening of the underlying continuum in the redder QSOs.

The mean redshift for the new KX QSOs in our survey is  $z = 2.50 \pm 0.50$ . This compares to a redshift range of  $z = 1.08\text{--}4.55$  and a mean of  $z = 2.05 \pm 0.71$  for the 23 X-ray selected sources from Akiyama et al. (2008) which comply with our KX selection and  $M_B$  absolute magnitude limit, but which were removed from our initial sample selection. As expected the redshift distributions for these two samples are statistically indistinguishable and the combined sample has a mean redshift of  $z = 2.30 \pm 0.81$ .

#### 3.2 QSO Surface Density

We can use our survey to place a lower limit on the number density of QSOs brighter than our effective magnitude limit of  $K_{tot} \leq 20$ . Correcting for the weighting in our spectroscopic sample selection suggests our KX selection would

TABLE 1.  
PROPERTIES OF NEW KX-SELECTED QSOs

ID	R.A. (J2000)	Dec.	$K_{tot}$	$(B - V)_{ap}$	$(V - J)_{ap}$	$(J - K)_{ap}$	$z$	$M_B$	$f_X^a$ (0.5–4.5 keV)	$L_X^b$ (2–10 keV)
UDS2074	02 17 03.86	−05 31 40.6	18.64	$−0.00 ± 0.01$	$1.47 ± 0.01$	$1.40 ± 0.14$	2.286	−24.2	$5.9 ± 0.9$	1.9
UDS5596	02 19 10.00	−05 29 30.8	18.62	$0.43 ± 0.01$	$1.22 ± 0.01$	$1.13 ± 0.16$	2.665	−24.2	$2.6 ± 0.8$	1.1
UDS7821	02 18 45.94	−05 28 06.5	18.47	$0.01 ± 0.01$	$1.39 ± 0.01$	$1.53 ± 0.14$	1.570	−23.2	$8.4 ± 0.9$	1.0
UDS10725*	02 18 50.17	−05 26 22.6	18.63	$0.60 ± 0.02$	$2.41 ± 0.02$	$1.61 ± 0.15$	1.979	−23.3	< 1.5	< 0.8
UDS15871	02 18 47.62	−05 23 19.9	19.95	$0.75 ± 0.01$	$1.08 ± 0.03$	$1.11 ± 0.26$	3.020	−23.1	$2.6 ± 0.5$	1.4
UDS17477	02 17 30.58	−05 22 22.9	19.08	$0.41 ± 0.01$	$0.90 ± 0.02$	$1.70 ± 0.18$	2.498	−23.3	$5.7 ± 0.6$	2.0
UDS23719*	02 18 27.47	−05 18 37.2	18.19	$0.83 ± 0.02$	$2.52 ± 0.02$	$1.88 ± 0.13$	2.988	−24.4	< 1.3	< 1.1
UDS25968	02 16 20.71	−05 17 18.7	18.85	$1.24 ± 0.01$	$1.36 ± 0.01$	$1.19 ± 0.14$	3.190	−23.7	$7.7 ± 1.2$	7.6
UDS34882	02 19 24.29	−05 11 49.6	18.66	$0.42 ± 0.01$	$1.19 ± 0.02$	$1.83 ± 0.10$	2.522	−23.4	$6.3 ± 1.3$	6.4
UDS34994	02 16 55.23	−05 11 46.7	19.50	$0.29 ± 0.01$	$1.04 ± 0.02$	$1.21 ± 0.19$	2.793	−23.4	$3.4 ± 0.7$	1.5
UDS66644	02 18 08.62	−04 53 54.6	18.35	$0.55 ± 0.01$	$1.48 ± 0.01$	$1.68 ± 0.12$	2.296	−23.8	< 0.9	< 0.6
UDS70628	02 18 40.26	−04 51 46.6	19.39	$0.34 ± 0.01$	$0.78 ± 0.03$	$1.74 ± 0.18$	2.550	−23.2	$6.2 ± 1.0$	2.3
UDS71490	02 17 13.13	−04 51 15.9	18.43	$0.40 ± 0.01$	$1.24 ± 0.02$	$1.41 ± 0.15$	2.504	−24.2	< 2.1	< 1.5
UDS80102	02 17 14.04	−04 46 12.6	18.70	$0.66 ± 0.01$	$1.69 ± 0.01$	$1.22 ± 0.15$	2.690	−24.0	$4.2 ± 0.6$	1.7
UDS86884*	02 17 35.95	−04 42 33.6	18.77	$1.17 ± 0.02$	$2.75 ± 0.02$	$1.32 ± 0.15$	3.292	−24.1	$1.7 ± 0.5$	1.4
UDS89180	02 17 32.87	−04 41 17.6	19.15	$0.34 ± 0.01$	$1.40 ± 0.02$	$1.10 ± 0.18$	1.907	−23.3	$3.8 ± 0.5$	0.7
UDS90590	02 16 47.28	−04 40 30.0	18.76	$0.28 ± 0.01$	$0.95 ± 0.02$	$1.46 ± 0.10$	1.728	−23.1	$7.7 ± 0.8$	1.5

**Table 1.** Typical errors are  $\pm 0.5''$  on positions,  $\pm 0.05$  on total  $K$ -band magnitudes,  $\pm 0.1$ – $0.3$  on  $M_B$  and  $\pm 0.001$  on  $z$ . All redshifts have  $Q=1$  except for those marked \* which have  $Q=2$ . a) units are  $10^{-15}$  erg s $^{-1}$  cm $^{-2}$ . b) units are  $10^{44}$  erg s $^{-1}$ .

have yielded more than 17 QSOs if we had observed all of the candidates (this does not include QSOs where the spectra failed to yield an ID). This correction implies 18.2 QSOs in our 0.572 degree $^2$  field.

To determine the total number density of QSOs in the field, we have to add in the 30  $M_B \leq -23.0$  QSOs brighter than  $K_{tot} = 20.0$  which were removed from our target list as they had existing spectroscopy from Akiyama et al. (2008). These include the 23 QSOs which comply with our KX and morphological selection, and a further seven which are not identified by the KX colour and morphology selections. Four of these seven are more extended (in  $R$ , and  $K$ ) than our FWHM cut, one falls outside the KX color region and two fall in regions with poor photometric coverage. Combining these two samples yields a surface density of  $\geq 85$  QSOs per degree $^{-2}$  brighter than  $K_{tot} = 20.0$ .

The main uncertainty in the estimate above is the incompleteness in our spectroscopic identifications, which is significant for  $V > 22$  sources. Correcting for this incompleteness is highly uncertain as it requires an assumption about the spectral properties of any undetected QSOs. Assuming that all of these systems exhibit strong emission lines would suggest little incompleteness in our identification of QSOs, leading to an actual surface density close to the limit quoted above. However, such an assumption is at odds with the spectral properties of even the detected QSOs (Fig. 3). An alternative approach is to assume that the incompleteness of the QSO sample is similar to the overall incompleteness of our identifications for the full spectroscopic sample at the same  $V$ -band magnitudes (i.e. that the incompleteness simply reflects continuum signal-to-noise in the spectra). Adopting this assumption we estimate a surface density of QSOs with  $K_{tot} \leq 20.0$  in our survey of 56 degree $^{-2}$  and correcting for our sampling and adding in the known X-ray selected QSOs, raises this to  $\sim 150$  degree $^{-2}$ .

Our limit on the QSO surface density are broadly consistent with the published limit of  $325_{-177}^{+316}$  deg $^{-2}$  at  $K \lesssim 19.5$  by Croom et al. (2001), based on the detection of 3 QSOs in a small 48 arcmin $^2$  field. As expected, our observed QSO surface density is significantly higher than that estimated at  $K \sim 15$  by Glikman et al. (2004, 2007), of just  $\sim 0.1$  deg $^{-2}$ . A more useful comparison is to the recently completed  $K$ -band QSO survey by Maddox et al. (2008). They surveyed 12.8 degree $^2$  to  $K = 17$  and determine a surface density of  $15.3 \pm 1.1$  deg $^{-2}$ , indicating that QSO counts increase roughly linearly with  $K$ -band flux fainter than  $K = 17$ .

In terms of theoretical predictions, Maddox & Hewett (2006) provide estimates for the number counts of QSOs in the  $K$ -band based on a standard model of the evolution of the QSO Luminosity Function, but with the addition of a model for the influence of host galaxy light on the apparent magnitudes of the QSOs. Their pure-QSO model (no contribution from the host galaxy) predicts  $\sim 100$  degree $^{-2}$  QSOs with  $M_B \leq -23.0$  QSOs and  $K \leq 20.0$ , while the inclusion of light from the host galaxy in their models increases this to  $\sim 110$  degree $^{-2}$ . We therefore conclude that our observational limits are consistent with the predicted number counts of QSOs in the  $K$ -band from Maddox & Hewett (2006) and depending upon the degree of incompleteness in our survey may support a modest contribution from the host galaxies in the  $K$ -band light from our QSO sample.

### 3.3 QSO Properties

We find a range of  $(B - K) = 2.5$ – $5.5$  for our QSO sample (Fig. 4), less than found for lower- $z$  QSOs (Glikman et al. 2004). This moderate range in colour likely reflects the limit imposed by our spectroscopic incompleteness which becomes substantial beyond  $V = 22$  (equivalent to  $K \sim 18$ ),

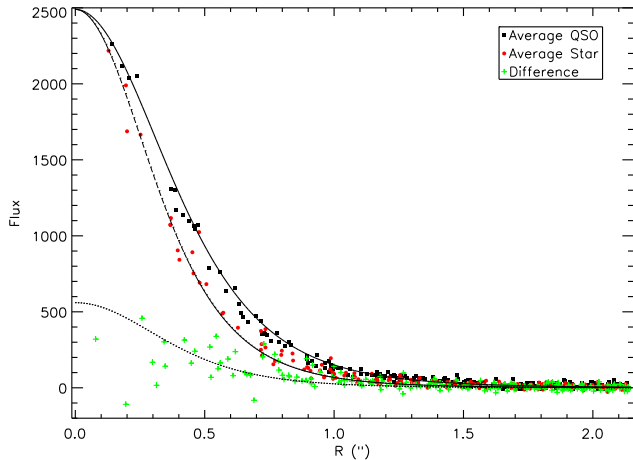


**Figure 5.** The radial  $K$ -band light profiles for the average QSO in our KX-selected sample and a spatially- and magnitude-matched sample of colour-selected stars. The measured FWHM from Moffat fits to the average QSO and star are  $0.80 \pm 0.05''$  and  $0.67 \pm 0.05''$  respectively, showing that the QSOs are on average more extended than nearby stars. Subtracting a scaled star from the composite QSO suggest the residual light comprises 25–40% of the light of the QSO, equivalent to  $K_{tot} \sim 20.3$ , and has an extent of several kpc. The profiles of the average QSOs which are redder and bluer than  $(B - K) = 3.5$  indicates that the bluer QSOs are more compact,  $0.75 \pm 0.05''$ , although this is not statistically significant.

with only the bluest QSOs having adequate  $V$ -band signal-to-noise for us to measure a redshift at  $K \sim 20$ . Nevertheless, we have 6/17 QSOs ( $\sim 35\%$ ) in our sample redder than the  $(B - K) = 3.5$ , frequently used to identify red QSOs (e.g. Jurek et al. 2008). Although we note that we have no examples of very red QSOs with  $(V - J) \geq 3$  in our AAOmega sample (Croom et al. 2001), again likely due to the incompleteness for fainter  $V$ -band sources in our spectroscopy, but such red QSOs do exist in the X-ray sample in this field.

The new KX-selected sample of QSOs in Fig. 4 displays a trend to redder  $(B - K)$  colours for higher redshift QSOs. This most likely reflects increasing absorption by the Ly $\alpha$  forest effecting the  $B$ -band emission of more distant QSOs (the X-ray sample exhibits a similar trend, Fig. 4).

We can exploit the high-quality multiwavelength data for the UDS region to investigate the properties of the QSOs we have discovered. Of our 17 new QSOs, 13 fall within  $5''$  of X-ray sources in the *XMM-Newton* catalogue of this field (Ueda et al. 2008) and we list their X-ray fluxes in Table 1. Indeed, we note that 31 sources from our spectroscopic sample of 426 objects are matched to the 952 sources in the X-ray catalog within  $5''$ , and that of the 13 of these X-ray sources which lie at  $z > 1.5$ , 12 appear in our KX QSO catalogue. The thirteenth was removed as the spectra were of too low quality. For the 13 X-ray detected QSOs we derive colours in the observed 0.5–4.5 keV band for these sources. For 12/13 their colours are consistent with no or little absorption, indicating that these are all type-1 AGNs. However, the X-ray color of UDS34882 appears hard in the 0.5–4.5 keV band, and suggests an absorbing column of  $N_H$  of  $2 \times 10^{23} \text{ cm}^{-2}$  (assuming a photon index of 1.8). This

source therefore appears to be a candidate of an “X-ray absorbed” QSO.

Comparing the redshift distributions of the X-ray undetected and detected subsamples in Table 1, we see that the X-ray undetected and detected QSOs have similar redshifts distributions ( $z = 2.44 \pm 0.18$  versus  $z = 2.52 \pm 0.15$ , where the errors are bootstrap estimates). Looking at the X-ray luminosities and limits of the detected and undetected QSOs, and comparing these to their optical absolute  $B$ -band magnitudes, it is clear that many of the X-ray detected QSOs lie close to the limits of the X-ray data and hence the X-ray undetected QSOs may represent the X-ray-faint wing of the distribution, rather than an intrinsically different population. This underlines the effectiveness of deep X-ray surveys for identifying QSOs.

We find that none of our 17 new QSOs has detectable radio emission brighter than  $100 \mu\text{Jy}$  at 1.4 GHz (Simpson et al. 2006), so they are all radio-quiet.

Finally, we have also compared the image profiles of the  $K$ -band light in the QSOs to nearby stars. We identify stars based on their  $VJK$  colours in Fig. 2 and select a subsample with the same range in  $K$ -band magnitudes and lying within  $120''$  of the QSOs. We stacked the images of 17 QSOs and comparison stars to produce composite profiles and we plot these in Fig. 5. This shows that the QSOs are more spatially extended in the  $K$ -band than nearby stars of similar magnitudes, with FWHM measured from Moffat fits of  $0.80 \pm 0.03''$  for the QSOs and  $0.67 \pm 0.03''$  for the stars. Subtracting a scaled star from the composite QSO image suggest the extended component of the  $K$ -band light comprises 25–40% of the light of the QSO, equivalent to  $K_{tot} \sim 20.3$ , and appears to have a spatial extent of  $\sim 2$ –5 kpc. The crude sizes and brightnesses of this component are similar to that measured from AO imaging of high-redshift QSO hosts (e.g. Falomo et al. 2008) and the fraction of the total light emitted in the restframe  $R$ -band is also similar to that seen in local QSOs (Maddox & Hewett 2006). Thus this extended component thus has many of the features expected for the QSO host galaxy (Maddox & Hewett 2006).

### 3.4 Foreground Galaxies

We show in Fig. 4 the colour distribution for the large sample of foreground galaxies identified in our survey. There are 302 galaxies in our AAOmega sample with  $Q=1$  spectra, their redshifts span  $z = 0.03$ –1.62 and a mean of  $z = 0.43 \pm 0.22$ . The spectral mix of this population includes sources whose spectra are best-fit by broad-line AGN (53), narrow-line AGN (13), narrow emission-line galaxy (23), absorption-line galaxy (75) and spiral galaxy (138) templates. The  $(B - K)$  colour distribution for these galaxies extends to very red colours,  $(B - K) \gtrsim 7$ , and show an upper envelope consistent with the expected colours of a non-evolving  $L^*$  E/S0 galaxy (Fig. 4).

Eleven of these foreground galaxies, at redshifts of  $z = 0.20$ –1.38, are matched to the *XMM-Newton* X-ray source catalogue (Ueda et al. 2008) within  $5''$ . Ten of these 11 have spectra which are best fit by broad-line (QSO) spectral templates, although their absolute restframe  $B$ -band luminosities are fainter than  $M_B \sim -23$ .

### 3.5 Improving the sample selection

Our identification of 17 new QSOs from spectroscopy of over 400 sources indicates a modest rate of return. This is mitigated somewhat by the fact that we removed from our input catalogue those QSOs already known from the existing spectroscopy of X-ray sources in this field. At best these would have doubled our success rate. Nevertheless, it is clear that even with the grasp of the AAOmega spectrograph a substantially larger future KX QSO survey would benefit from reducing the contamination from foreground compact galaxies.

We have therefore investigated two routes we could have potentially improved the yield of QSOs in our spectroscopic survey: 1) reducing the limit on object compactness and 2) including a cut based on  $(B - V)$  colour. To illustrate this we show the distribution of  $(B - V)$  colours and  $R$ -band FWHM for the new QSOs from our AAOmega sample, the X-ray selected QSOs in this field and the contaminating population of foreground galaxies in Fig. 6.

A reduction in contamination could be achieved by adopting a  $(B - V) \leq 1.2$  cut, which reduces contamination by  $\sim 30\%$  but at the cost of potentially removing red QSOs and those at higher-redshifts. Similarly using  $B$ -band FWHM (cut at  $\leq 1.1''$ ) can reduce contamination by  $\sim 40\%$ . Combining these two selections would reduce contamination by  $\sim 60\%$  overall and result in a final QSO yield of 10%.

Adopting a more rigorous limit on FWHM, say  $\leq 1.0''$ , would significantly reduce the contamination, by  $\sim 80\%$ , at the cost of losing a small number of QSOs with resolved hosts ( $\sim 10\%$ ). For certain experiments, especially those targeting high-redshift QSOs, such an approach might be appropriate as the host galaxies of such systems are unlikely to be individually detected and in this mode KX-selection would yield very high completeness.

We caution that our sample is far from ideal for identifying an optimal selection as the selection criteria will be tuned for selecting QSOs similar to those that we have found: at  $z \lesssim 3.5$  and relatively blue. A better training set would be provided by a more complete spectroscopic sample, including near-infrared spectroscopy with FMOS, to overcome the bias towards optically bright QSOs in the current sample. We also note that further detailed studies of the contaminating population may be a productive route to identify criteria to remove them from the KX QSO sample.

## 4 CONCLUSIONS

We present the results from a pilot survey for QSOs in the UKIDSS UDS field. We employ the KX selection method of Warren et al. (2000) to select a sample of faint candidate QSOs from the very deep optical and near-infrared imaging available for this field. We have then followed up these sources with the 400-fibre AAOmega spectrograph in service time on the AAT to identify the high-redshift QSOs in the  $\sim 700$  KX-selected compact sources in our catalogue. We identify 17 QSOs with  $M_B \leq -23$  in this pilot survey. Supplemented by existing spectroscopy of X-ray selected AGN in this field (Akiyama et al. 2008) this yields a combined QSO sample with a surface density of  $\sim 85\text{--}150 \text{ degree}^{-2}$  at  $K_{tot} \leq 20$  (where the range reflects the uncertainty in the

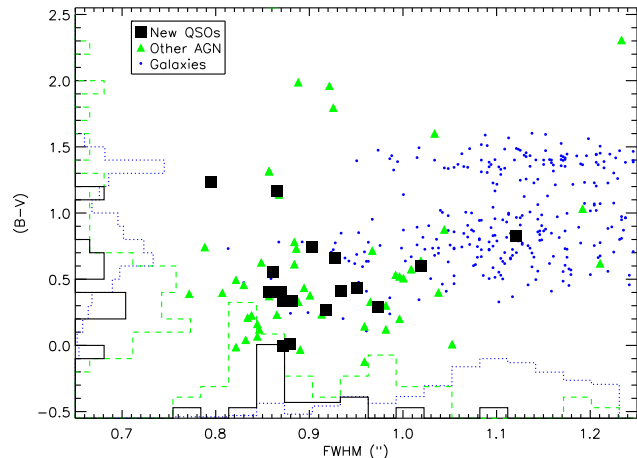


**Figure 6.**  $(B - V)$  versus FWHM in the  $R$ -band for spectroscopically identified QSOs in the UKIDSS UDS (both the X-ray and KX-selected) and the contaminating population of foreground galaxies. We plot histograms showing the distribution in  $(B - V)$  colour and FWHM for each of the three samples: new KX QSOs (solid), existing AGN (dotted) and galaxies (dashed). These distributions illustrate the challenge of isolating the QSO populations from the compact, faint galaxies. We conclude that complete samples of QSOs cannot be efficiently constructed from simple selection based on image compactness or colour, although more stringent limits on image compactness would yield significant reductions in contamination, at relatively modest cost in terms of incompleteness.

spectroscopic incompleteness in our sample). This sample is roughly  $4\times$  deeper than previous KX-selected surveys over comparable areas (Jurek et al. 2008) and  $40\times$  larger than the previous surveys at similar  $K$ -band depth (Croom et al. 2001).

We have used the good image quality of the UKIDSS UDS data to create composite  $K$ -band images of our QSO sample and a matched sample of stars. The light profiles of the two composites show that the QSOs are more spatially extended. The extended component comprises some 25–40% of the total  $K$ -band light of the QSO and has a spatial extent of  $\sim 2\text{--}5$  kpc. This most likely represents the host galaxy of the QSO.

We analyse our sample to attempt to refine the KX selection technique to reduce the considerable contamination by low redshift,  $z \lesssim 0.6$ , compact galaxies. We find that colour or morphological selections focusing on bluer passbands (e.g. an additional  $(B - V)$  cut or limits on image FWHM in the  $B$ -band) would reduce the contamination in our parent sample. However, these approaches would bias the resulting sample against redder or higher-redshift QSOs and so may not be desirable for certain applications where completeness is important. Alternatively, if the goal is to maximise the number of high-redshift QSOs detected, then the KX selection using a more conservative FWHM limit,  $\leq 1.0''$  in the case of the  $0.8''$ -FWHM UDS imaging, can significantly reduce the foreground contamination while at the same time yielding high completeness ( $\sim 90\%$ ).

From our sample we cull a subsample of  $\sim 21$  QSOs at  $z > 2.5$  and  $V < 23$  which are suitable for an absorption line study (see Adelberger et al. 2005) employing deep blue spec-



troscopy with VIMOS on VLT. In addition, the full sample of QSOs (including those at lower redshifts) provide a map of the distribution of rapidly growing black holes within our survey volume, enabling us to relate these to the growth of mass-selected samples of galaxies and the surrounding absorption-line systems. These luminous AGN are expected to have measurable feedback effects on the gas – an issue of great interest to current models of galaxy formation (in which such forms of feedback are an essential part, Bower et al. 2006).

## ACKNOWLEDGMENTS

We thank the members of the UDS Working Group, in particular Chris Simpson, and Natasha Maddox, Paul Hewett and Dave Alexander for help and useful discussions. We thank the Referee for their clear and insightful report, which helped improve the accuracy and presentation of this paper. IRS acknowledges support from the Royal Society. AMS acknowledges support from STFC. This work is based in part on data obtained as part of the UKIRT Infrared Deep Sky Survey. We acknowledge the contributions of the staff of UKIRT to the implementation UKIDSS survey and the Cambridge Astronomical Survey Unit and the Wide Field Astronomy Unit in Edinburgh for processing the UKIDSS data. The United Kingdom Infrared Telescope is operated by the Joint Astronomy Centre on behalf of the Science and Technology Facilities Council of the U.K. This paper uses data obtained through the Service Programme at the Anglo-Australian Telescope. This work was based in part on observations made with the Anglo-Australian Telescope. We warmly thank all the present and former staff of the Anglo-Australian Observatory for their work in building and operating the 2dF and AAOmega facilities.

## REFERENCES

- Adelberger, K., Shapley, A.E., Steidel, C.C., Pettini, M., Erb, D.K., Reddy, N.A., 2005, *ApJ*, 629, 636
- Akiyama, M., et al., 2008, in prep.
- Almaini, O., et al., 2008, in prep.
- Blanton, M.R., Roweis, S., 2007, *AJ*, 133, 734
- Bower, R.G., Benson, A.J., Malbon, R., Helly, J.C., Frenk, C.S., Baugh, C.M., Cole, S., Lacey, C.G., 2006, *MNRAS*, 370, 645
- Cannon, R., Drinkwater, M., Edge, A., Eisenstein, D., Nichol, R., Outram, P., Pimblett, K., de Propris, R., Roseboom, I., 2006, *MNRAS*, 372, 425
- Cirasuolo, M., McLure, R.J., Dunlop, J.S., Almaini, O., Foucaud, S., Smail, I., Sekiguchi, K., et al., 2007, *MNRAS*, 380, 585
- Colless, M.M., Dalton, G., Maddox, S., Sutherland, W., Norberg, P., Cole, S., Bland-Hawthorn, J., Bridges, T., et al., 2001, *MNRAS*, 328, 1039
- Croom, S.M., Warren, S.J., Glazebrook, K., 2001, *MNRAS*, 328, 150
- Croom, S.M., et al., 2001, *MNRAS*, 322, L29
- van Dokkum, P., 2001, *PASP*, 113, 1420
- Falomo, R., Treves, A., Kotilainen, J., Scarpa, R., Uslenghi, M., 2008, *ApJ*, 673, 694
- Foucaud, S., Almaini, O., Smail, I., Conselice, C.J., Lane, K. P.; Edge, A.C., Simpson, C., Dunlop, J.S., et al., 2007, *MNRAS*, 376, L20
- Furusawa, H., Kosugi, G., Akiyama, M., Takata, T., Sekiguchi, K., Tanaka, I., Iwata, I., Kajisawa, M., et al., 2008, *ApJS*, 176, 1
- Glikman, E., Gregg, M.D., Lacy, M., Helfand, D.J., Becker, R.H., White, R.L., 2004, *ApJ*, 607, 60
- Glikman, E., Helfand, D.J., White, R.L., Becker, R.H., Gregg, M.D., Lacy, M., 2007, *ApJ*, 667, 673
- Jurek, R.J., Drinkwater, M.J., Francis, P.J., Pimblett, K.A., 2008, *MNRAS*, 383, 673
- Lane, K., Almaini, O., Foucaud, S., Simpson, C., Smail, I., McLure, R. J., Conselice, C.J., Cirasuolo, M., et al., 2007, *MNRAS*, 379, L25
- Lawrence, A., Warren, S.J., Almaini, O., Edge, A.C., Hambly, N.C., Jameson, R.F., Lucas, P., et al., 2007, *MNRAS*, 379, 1599
- Maddox, N., Hewett, P.C., 2006, *MNRAS*, 367, 717
- Maddox, N., Hewett, P.C., Warren, S.J., Croom, S.M., 2008, *MNRAS*, 386, 1605
- Morris, S., Januzzi, B., 2006, 367, 1261
- Prescott, M.K.M., Impey, C.D., Cool, R.D., Scoville, N.Z., 2006, *ApJ*, 644, 100
- Saunders, W., Bridges, T., Gillingham, P., Haynes, R., Smith, G.A., Whittard, J.D., Churilov, V., Lankshear, A., et al., 2004, *SPIE*, 5492, 389
- Sharp, R., et al., 2002, 337, 1153
- Sharp, R., Saunders, W., Smith, G., Churilov, V., Correll, D., Dawson, J., Farrel, T., Frost, G., et al., 2006, *SPIE*, 6269, 14
- Simpson, C., Martinez-Sansigre, A., Rawlings, S., Ivison, R., Akiyama, M., Sekiguchi, K., Takata, T., Ueda, Y., Watson, M., 2006, *MNRAS*, 372, 741
- Smith, G.A., Saunders, W., Bridges, T., Churilov, V., Lankshear, A.,; Dawson, J., Correll, D., et al., 2004, *SPIE*, 5492, 410
- Ueda, Y., et al., 2008, in prep
- Warren, S., Hewett, P.C., Foltz, C.B., 2000, *MNRAS*, 312, 827
- Warren, S., Hambly, N.C., Dye, S., Almaini, O., Cross, N.J.G., Edge, A.C., Foucaud, S., Hewett, P.C., et al., 2007, *MNRAS*, 375, 213